Article

Journal of
Nanoscience and Nanotechnology
Vol. 14, 9670–9679, 2014
www.aspbs.com/jnn

On the Etching Characteristics and Mechanisms of HfO_2 Thin Films in $CF_4/O_2/Ar$ and $CHF_3/O_2/Ar$ Plasma for Nano-Devices

Nomin Lim[1], Alexander Efremov[2], Geun Young Yeom[3], and Kwang-Ho Kwon[1,*]

[1] *Department of Control and Instrumentation Engineering, Korea University, Sejong 339-700, South Korea*
[2] *Department of Electronic Devices and Materials Technology, State University of Chemistry and Technology, 7 F. Engels St., 153000 Ivanovo, Russia*
[3] *Department of Advanced Materials Science and Engineering, Sungkyunkwan University, Suwon 440-746, South Korea*

The study of etching characteristics and mechanisms for HfO_2 and Si in $CF_4/O_2/Ar$ and $CHF_3/O_2/Ar$ inductively-coupled plasmas was carried out. The etching rates of HfO_2 thin films as well as the HfO_2/Si etching selectivities were measured as functions of Ar content in a feed gas (0–50% Ar) at fixed fluorocarbon gas content (50%), gas pressure (6 mTorr), input power (700 W), bias power (200 W), and total gas flow rate (40 sccm). Plasma parameters as well as the differences in plasma chemistries for CF_4- and CHF_3-based plasmas were analyzed using Langmuir probe diagnostics and 0-dimensional plasma modeling. It was found that, in both gas systems, the non-monotonic (with a maximum at about 15–20% Ar) HfO_2 etching rate does not correlate with monotonic changes of F atom flux and ion energy flux. It was proposed that, under the given set of experimental conditions, the HfO_2 etching process is affected by the factors determining the formation and decomposition kinetics of the fluorocarbon polymer layer. These factor are the fluxes of CF_x ($x = 1, 2$) radicals, O atoms and H atoms.

Keywords: HfO_2, CF_4- and CHF_3-Based Plasmas, Etching Rate, Etching Mechanism, Polymerization.

1. INTRODUCTION

During last years, many new materials have been involved in the micro- and nano-electronics technology aimed at developing new devices as well as improving characteristics of conventional ones. Particularly, in the dynamic random access memory (DRAM) technology, the evident trend is the replacement of the conventional low-k dielectric materials (SiO_2, Si_3N_4) for the high-k dielectrics, such as Ta_2O_5, Y_2O_3, HfO_2, ZrO_2, $BaTiO_3$, and $SrTiO_3$.[1,2] Among these materials, HfO_2 is a promising candidate for nano devices because of its dielectric constant of about 20 and relatively large bandgap energy of 5.7 eV.[3,4] Furthermore, the HfO_2 thin films produced by the atomic layer deposition (ALD) method are in good compartibility with the neighborhood technological steps because of low deposition temperature and superior step coverage. Therefore, the development and optimization of the dry patterning process for HfO_2 thin films for developing nano devices is an important task to be solved for obtaining stable and advanced device characteristics.

Currently, there are many published works on the investigation of the HfO_2 etch process in fluorine-based,[3–9] chlorine-based,[3,6,7,9–12] bromine-based[6,10,13] and hydrogen-based[3] gas chemistries. The results of these works can be summarised as follows: (1) The chemical enhancement of the HfO_2 etching rate over the pure ion etching in Ar plasma is maximum for the Cl- and Br-based gas chemisties and minimum for the fluorine-based ones. This fact is in consistence with the volatilities of the corresponding reaction products. Particularly, in our earlier work[12] we have found that the HfO_2 etching rate in Cl_2 plasma about 10 times higher than that in Ar plasma under the one and the same input procees conditions. At the same time, the substitution of Ar by C_4F_8 increases the HfO_2 etching rate by less than 2 times.[3,8] (2) The addition of BCl_3 to any plasma system increases the HfO_2 etch rate as have been found earlier for many metal oxide materials.

*Author to whom correspondence should be addressed.

 1533-4880/2014/14/9670/010 doi:10.1166/jnn.2014.10171

The authors of Ref. [15] attributed such effect to the chemical activity of BCl_x radical which liberate the oxygen from the oxide and thus, support the halogenisation of Hf itself. (3) The use of the fluorocarbon-based chemistries was found to be preferable for the cases where the etching selectivity is the key issue.[5–7] An increase in the C/F ratio improves the HfO_2/Si etching selectivity, but simultaneosly enriches the surface by the polymer residues.[5] The dilution of the fluorocarbon gas by Ar at constant gas pressure results in the non-monotonic (with a maximum) HfO_2 etching rate. Such effect have repeatedly been obtained for C_4F_8 /Ar[9] and CF_4/Ar[16] plasmas.

Unfortunately, the majority of works dealing with the fluorine-based gas chemisties were simply focused on the dependencies of HfO_2 etching rates on operating parameters in order to obtain better etching selectivities over varions under- or over-laying materials. On this backgroung, the relationships between etching rates, plasma parameters and fluxes of plasma active species received much less attention. In fact, this menas that the HfO_2 etching mechanism have not been explored in details. Such situation retards the development and optimization of the HfO_2 dry etching technology for developing nano devices.

In this work, we carried out the comparative study of etching characteristics and mechanisms for HfO_2 and Si in $CF_4/O_2/Ar$ and $CHF_3/O_2/Ar$ inductively-coupled plasmas. These two gas system have never been compared directly for HfO_2 etching process in the terms of plasma compositions and etching mechanisms. The interest to silicon is because it is frequently used as the substrate material for the deposition of HfO_2 thin films. Therefore, it was examined only in order to obtain the etching selectivity over HfO_2. The choice of the oxygen-containing fluorocarbon (FC) gas chemistry is because of the well known effect of increasing rate of the chemical etching pathway for Si and SiO_2 in a presence of O_2 in a feed gas.[17,18] We would like to mention also that, for both CF_4- and CHF_3-based plasma, the effect of O_2 on plasma parameters and etching rates is well studied only for the binary (FC/O_2) gas mixtures where an increase in the O_2 fraction is accompanied by a proportionally decreasing FC gas fraction. In the free-component gas systems, one can fix the fraction of FC gas, but change only the ratio between O_2 and Ar. It is clear that, since the composition of the feed gas is different compared with simple FC/O_2 mixture, some principal differences in plasma parameters and etching mechanisms can take place. That is why, the relationships between plasma parameters, composition and etching rates for the three- component FC/O_2/Ar gas mixtures with a constant fraction of the FC gas need additional investigations.

2. EXPERIMENTAL PART

2.1. Experimental Setup and Procedures

HfO_2 thin films were deposited on *p*-type Si (100) substrates by the atomic layer deposition (ALD) technique. Before the deposition, the Si substrates were wet etched in HF and rinsed in deionized water in order to remove native oxide. The deposition process consisted of periodic exposures of the substrates to the vapor of $HfCl_4$. Each of the exposures was followed by purging with pure nitrogen (AGA, 99.999%), an exposure to H_2O vapor, and another purging with nitrogen gas. The exposure and purging periods each lasted 2 s. $HfCl_4$ (Sigma-Aldrich, 98%) was evaporated from a cell that was kept in the flow of the carrier gas (N_2). The samples were immediately loaded into the reactor and ALD was performed at temperatures between 70 and 130 °C.

Both etching and plasma diagnostics experiments were performed in planar inductively coupled plasma (ICP) reactor. The reactor had a cylindrical ($r = 15$ cm) chamber made from the anodized aluminum. The 5-turns copper coil with a diameter of 29 cm was connected to the 13.56 MHz power supply and located above the 10 mm thick-horizontal quartz window on the top side of the chamber. A distance (l) between the window and the bottom electrode used as a substrate holder was 12.8 cm. The bottom electrode was connected to 12.56 MHz power supply to maintain a negative dc bias voltage (U_{dc}). The temperature of the bottom electrode was stabilized at 17 °C using the water-flow cooling system.

The experiments were performed at fixed total gas flow rate ($q = 40$ sccm), gas pressure ($p = 6$ mTorr), bias power ($W_{dc} = 200$ W) and input power ($W_{inp} = 700$ W). The initial compositions of $CF_4/O_2/Ar$ or $CHF_3/O_2/Ar$ mixtures were set by adjusting the flow rates of corresponding individual gases. Particularly, the flow rates of fluorocarbons (FC) q_{FC} was always fixed at 20 sccm while O_2 and Ar were mixed with various ratios within $q_{O_2} + q_{Ar} = 20$ sccm. Accordingly, in all experiments the fractions of CF_4 or CHF_3 in the initial gas mixture $y_{FC} = q_{FC}/q$ were kept as 0.5, and the remaining half was composed by the different amounts of O_2 and Ar. Therefore, the variation of Ar content in a feed gas in the range of 0–50% ($y_{Ar} =$ 0–0.5) corresponds to the transition between FC/O_2 and FC/Ar gas systems.

For etching experiments, the samples with the size of about 2×2 cm^2 were placed in the center of the bottom electrode. The HfO_2 and Si etched depths were measured using a surface profiler (Alpha-step 500, Tencor). For this purpose, we developed the line striping of the PR (AZ1512, positive) with the line width/spacing ratio of 2 μm/2 μm. The initial thickness of the PR layer was about 1.5 μm.

Plasma diagnostics was carried out by double Langmuir probe (LP) (DLP2000, Plasmart Inc.). The probes were installed through a hole on the sidewall of the reactor chamber at 5.7 cm above the bottom electrode and centered in a radial direction. The output data were the electron temperature (T_e), ion current density (J_+), floating potential (U_f) and total positive ion density (n_+).

Table I. Reaction set for modeling of neutral species chemistry in $CF_4/O_2/Ar$ and $CHF_3/O_2/Ar$ plasmas.

			Rate coefficient [cm^3/s]		
	Process	ε_{th} [eV]	A	B	C
R1	$CHF_3 + e = F + CHF_2 + e$	13.00	1.19×10^{-16}	1.317	1.38×10^{5}
R2	$CHF_3 + e = H + CF_3 + e$	11.00	3.96×10^{-17}	1.642	1.04×10^{5}
R3	$CHF_3 + e = HF + CF_2 + e$	23.60	3.63×10^{-14}	1.076	2.63×10^{5}
R4	$CHF_2 + e = CHF + F + e$	4.75	1.19×10^{-16}	1.317	1.38×10^{5}
R5	$CHF_2 + e = H + CF_2 + e$	2.71	3.96×10^{-17}	1.642	1.04×10^{5}
R6	$CHF + e = H + CF + e$	3.30	9.31×10^{-9}	0.204	11.42
R7	$CF_4 + e = CF_3 + F + e$	5.60	1.38×10^{-8}	0	16
R8	$CF_4 + e = CF_2 + 2F + e$	9.50	2.22×10^{-10}	0.99	14.77
R9	$CF_4 + e = CF_3^+ + F + 2e$	15.9	9.36×10^{-8}	0	20.4
R10	$CF_3 + e = CF_2 + F + e$	3.80	6.48×10^{-8}	−0.959	11.25
R11	$CF_2 + e = CF + F + e$	5.40	8.11×10^{-9}	0.386	8.739
R12	$CF_2 + e = C + 2F + e$	11.00	1.39×10^{-8}	−1.164	49.87
R13	$CF + e = C + F + e$	5.60	1.63×10^{-8}	−0.002	13.05
R14	$HF + e = H + F + e$	5.85	3.63×10^{-8}	−0.313	13.14
R15	$F_2 + e = 2F + e$	4.34	1.08×10^{-8}	−0.296	4.464
R16	$H_2 + e = 2H + e$	4.34	1.08×10^{-8}	−0.296	4.464
R17	$CH + e = C + H + e$	4.34	1.08×10^{-8}	−0.296	4.464
R18	$O_2 + e = 2O + e$	6.40	1.52×10^{-9}	0	4.15
R19	$O_2 + e = O + O(1d) + e$	8.57	2.04×10^{-8}	0	8.18
R20	$CO_2 + e = CO + O + e$	13.50	1.87×10^{-8}	0	13.89
R21	$CO + e = C + O + e$	13.50	1.87×10^{-8}	0	13.89
R22	$O + e = O(1d) + e$	1.97	4.47×10^{-9}	0	2.29
R23	$FO + e = F + O + e$	4.30	6.16×10^{-9}	0	4.30
R24	$CFO + e = CO + F + e$	5.40	8.11×10^{-9}	0.386	8.739
R25	$CF_2O + e = CFO + F + e$	3.80	6.48×10^{-8}	−0.959	11.25
R26	$CHF_3 + F = HF + CF_3$	1.58×10^{-13}			
R27	$CHF_3 + H = H_2 + CF_3$	1.60×10^{-19}			
R28	$CHF_2 + F = HF + CF_2$	3.16×10^{-11}			
R29	$CHF_2 + H = HF + CHF$	3.22×10^{-10}			
R30	$CHF_2 + H = CF_2 + H_2$	3.20×10^{-14}			
R31	$CHF_2 + CF_3 = CHF_3 + CF_2$	1.58×10^{-12}			
R32	$CHF_2 + O = CF_2O + H$	1.05×10^{-11}			
R33	$CHF + F = HF + CF$	3.25×10^{-11}			
R34	$CHF + H = HF + CH$	3.10×10^{-10}			
R35	$CHF + O = HF + CO$	3.25×10^{-11}			
R36	$F_2 + CF_3 = CF_4 + F$	6.31×10^{-14}			
R37	$F_2 + CF_2 = CF_3 + F$	7.94×10^{-14}			
R38	$F_2 + CF = CF_2 + F$	3.98×10^{-12}			
R39	$F_2 + H = HF + F$	8.20×10^{-12}			
R40	$F_2 + O(1d) = FO + F$	7.94×10^{-12}			
R41	$F_2 + CFO = CF_2O + F$	5.01×10^{-14}			
R42	$CF_3 + F = CF_4$	1.00×10^{-12}			
R43	$CF_3 + H = CF_2 + HF$	7.94×10^{-11}			
R44	$CF_3 + O = CF_2O + F$	3.16×10^{-11}			
R45	$CF_3 + O(1d) = CF_2O + F$	3.16×10^{-11}			
R46	$CF_2 + F = CF_3$	4.17×10^{-13}			
R47	$CF_2 + H = HF + CF$	3.20×10^{-11}			
R48	$CF_2 + O = CFO + F$	3.16×10^{-11}			
R49	$CF_2 + O(1d) = CFO + F$	3.16×10^{-11}			
R50	$CF_2 + O = CO + 2F$	3.98×10^{-12}			
R51	$CF_2 + O(1d) = CO + 2F$	3.98×10^{-12}			
R52	$CF + F = CF_2$	5.01×10^{-15}			
R53	$CF + H = C + HF$	1.20×10^{-11}			
R54	$CF + O = CO + F$	6.31×10^{-11}			
R55	$CF + O(1d) = CO + F$	2.00×10^{-11}			
R56	$CF + O_2 = CFO + O$	3.16×10^{-11}			
R57	$CH + HF = CF + H_2$	3.23×10^{-11}			
R58	$CH + O = CO + H$	1.06×10^{-10}			
R59	$CH + F = C + HF$	1.02×10^{-12}			
R60	$H_2 + F = HF + H$	1.60×10^{-11}			

Table I. Continued.

	Process	Rate coefficient [cm^3/s] ε_{th} [eV]	A	B	C
R61	$FO + O = F + O_2$	2.51×10^{-11}			
R62	$FO + O(1d) = F + O_2$	5.01×10^{-11}			
R63	$FO + FO = 2F + O_2$	2.51×10^{-12}			
R64	$2FO = F_2 + O_2$	2.51×10^{-16}			
R65	$CFO + CF_3 = CF_4 + CO$	1.00×10^{-11}			
R66	$CFO + CF_3 = CF_2O + CF_2$	1.00×10^{-11}			
R67	$CFO + CF_2 = CF_3 + CO$	3.16×10^{-13}			
R68	$CFO + CF_2 = CF_2O + CF$	3.16×10^{-13}			
R69	$CFO + O = CO_2 + F$	1.00×10^{-10}			
R70	$CFO + O(1d) = CO_2 + F$	1.00×10^{-10}			
R71	$2CFO = CF_2O + CO$	1.00×10^{-11}			
R72	$CFO + F = CF_2O$	7.94×10^{-11}			
R73	$CF_2O + O(1d) = F_2 + CO_2$	2.00×10^{-11}			
R74	$C + O_2 = CO + O$	1.58×10^{-11}			
R75	$CO + F = CFO$	1.29×10^{-11}			
R76	$F = F(s) + CHF_2 = CHF_3$				
	$+ CHF = CHF_2$				
	$+ CF_3 = CF_4$				
	$+ CF_3 = CF_4$				
	$+ CF_2 = CF_3$				
	$+ CF = CF_2$				
	$+ F = F_2$				
	$+ C = CF$				
	$+ O = FO$				
	$+ H = HF$	$f(\gamma), \gamma = 0.05$			
R77	$H = H(s) + F = HF$				
	$+ C = CH$				
	$+ H = H_2$				
	$+ CF_3 = CHF_3$				
	$+ CF_2 = CHF_2$				
	$+ CF = CHF$	$f(\gamma), \gamma = 0.05$			
R78	$CF_3 = CF_3(s) + F = CF_4$				
	$+ H = CHF_3$	$f(\gamma), \gamma = 0.05$			
R79	$CF_2 = CF_2(s) + F = CF_3$				
	$+ H = CHF_2$				
	$+ O = CF_2O$	$f(\gamma), \gamma = 0.1$			
R80	$CF = CF(s) + F = CF_2$				
	$+ H = CHF$				
	$+ O = CFO$	$f(\gamma), \gamma = 0.1$			
R81	$C = C(s) + F = CF$				
	$+ H = CH$				
	$+ O = CO$	$f(\gamma), \gamma = 1$			
R82	$O = O(s) + O = O_2$				
	$+ F = FO$				
	$+ C = CO$				
	$+ CF = CFO$				
	$+ CF_2 = CF_2O$	$f(\gamma), \gamma = 0.1$			
R83	$O(1d) = O$	$f(\gamma), \gamma = 1$			
R84	$CF_3^+ = CF_3$	v/d_c, where $v \approx \sqrt{eT_e/m_i}$ and $d_c = 0.5rl/(rh_l + lh_r)$			

Note: The units for rate coefficients of R1–R75 are cm^3/s. When calculating the rate coefficients for R1–R5, the electron temperature is substituted in [K], not in [eV].

The treatment of I–V curves was based on the Johnson & Malter's double probes theory[19] and the Allen-Boyd-Reynolds (ABR) approximation[20] for the ion saturation current density without accounting for negative ions. All these assume $J_+ \approx 0.61en_+v$, where v is the ion Bohm velocity. Earlier, it was shown that such an approach works not bad even for more electronegative plasmas, for example, for the Cl_2-bàsed ones.[21, 22]

2.2. Plasma Modeling

In order to obtain the data on densities and fluxes of plasma active species, we used a simplified

zero-dimensional model with Maxwellian electron energy distribution function (EEDF) and with the experimental data on T_e and n_+ as input parameters.[21,22] Though the real EEDFs are not exactly Maxwellian, such simplification for both the CF_4- and CHF_3-based low-pressure ($p < 50$ mTorr) ICPs provides the reasonable agreement between the results of plasma diagnostics and modeling.[22–24]

The transition from n_+ to electron density (n_e) was provided by the steady-state equation of chemical kinetics for negative ions

$$n_e \sum k_{\mathrm{da},j} n_j = k_{ii} n_+ n_-, \qquad (1)$$

which was solved with accounting for the quasi-neutrality condition $n_+ = n_- + n_e$. The rate coefficients of dissociative attachment k_{da} for neutral species with partial densities of n were taken from Refs. [24–27] as functions of T_e in a form of $k = AT_e^B \exp(-C/T_e)$. The ion–ion recombination rate coefficient $k_{ii} = 1 \times 10^{-7}$ cm^3/s was assumed to be the same for all types of positive and negative ions.[24,26]

The steady-state ($dn/dt = 0$) densities of neutral species were obtained from the system of chemical kinetics equations in a general form of $R_F - R_D = (k_s + 1/\tau_R)n$, where R_F and R_D are the volume-averaged formation and decay rates in bulk plasma for a given type of species, k_S is the first-order heterogeneous decay rate coefficient, and $\tau_R = \pi r^2 lp/q$ is the residence time. The list of the processes included in the model is given in Table I. The rate coefficients for electron impact reactions (R1–R25) were also calculated using the fitting expressions of $k = AT_e^B \exp(-C/T_e)$.[24–27] The rate coefficients for R26–R75 were taken from Refs. [25,28,29] for the gas temperature (T) of 700 K. The last was assumed to be independent on the variable operating parameters. The rate coefficients for heterogeneous loss of atoms and radicals R76–R83 were taken similarly to Ref. [21] as

$$k_S = [(\Lambda^2/D) + (2r/\gamma v_T)]^{-1}, \qquad (2)$$

where D is the effective diffusion coefficient, γ is the sticking probability,[24,26] $\Lambda^{-2} = (2.405/r)^2 + (\pi/l)^2$ is the diffusion length, and $v_T = (8k_B T/\pi m)^{1/2}$. All reaction pathways between the adsorbed (marked by the "s" index) and gaseous species inside R76–R83 were assumed to be of equal probabilities. The rate coefficients for heterogeneous loss of ions R84 were calculated as $k_S = v/d_c$, where $d_c = 0.5rl/(rh_l + lh_r)$. The correction factors for axial h_l and radial h_r sheath sizes are given by the low pressure diffusion theory.[29]

3. RESULTS AND DISCUSSION

3.1. Etching Rates and Selectivities

From Figure 1(a), it can be seen that, as the Ar content in both $CF_4/O_2/Ar$ and $CHF_3/O_2/Ar$ gas mixtures increases from 0–50% (i.e., as the transition from FC/O_2 to FC/Ar system takes place) the HfO_2 etching rates show the similar non-monotonic behaviors with a maximums at 15–20% Ar. In the $CHF_3/O_2/Ar$ plasma, the maximum etching rate (∼14.3 nm/min) is about 1.7 times higher than those for CHF_3/O_2 and CHF_3/Ar gas systems. In the $CF_4/O_2/Ar$ plasma, the maximum etching rate (∼18.3 nm/min) exceeds by 60% the etching rate in CF_4/Ar gas mixture, but appears to be only by 45% higher than the etching rate in the CF_4/O_2 gas system. Therefore, the $CF_4/O_2/Ar$ gas system shows the bigger gap in the etching rates between the completely oxygenated (50% O_2+ 0% Ar) and non-oxygenated (0% O_2+ 50% Ar) plasmas.

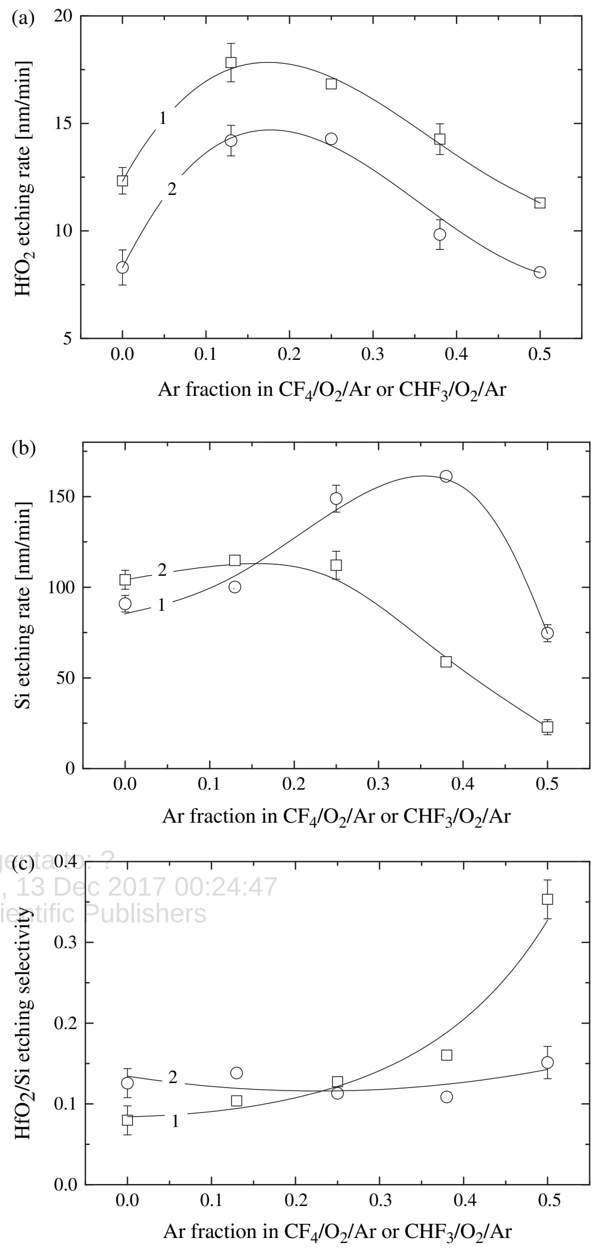

Figure 1. Etching rates and selectivities in $CF_4/O_2/Ar$ (1) and $CHF_3/O_2/Ar$ (2) plasmas at $W_{\mathrm{inp}} = 700$ W, $W_{\mathrm{dc}} = 200$ W and $p = 6$ mTorr: (a) HfO_2 etching rate; (b) Si etching rate; (c) HfO_2/Si etching selectivity.

In spite of the previous case, the etching behavior of Si is different in $CF_4/O_2/Ar$ and $CHF_3/O_2/Ar$ plasmas under one and the same operating conditions. As can be seen from Figure 1(b), as the $CF_4/O_2/Ar$ is reached by Ar, the Si etching rate increase from 91 nm/min (50% CF_4+ 50% O_2) up to about 161 nm/min (50% CF_4+ 10% O_2+ 40% Ar). The furthermore increase in Ar content in a feed gas and the transition to the 50% CF_4+ 50% Ar gas mixture lowers Si etching rate to the level of 75 nm/min. In the $CHF_3/O_2/Ar$ plasma, the dependence of Si etching rate on the Ar fraction in a feed gas has no evident maximum, but shows a kind of saturation region up to 25% Ar. Then, the furthermore increase in Ar content and the transition to the 50% CHF_3+ 50% Ar gas mixture lowers Si etching rate to the level of 23 nm/min. Therefore, in the non-oxygenated plasmas, the CF_4-based gas chemistry provides more than 3 times higher Si etching rate compared with CHF_3-based plasmas.

The quite close non-monotonic behaviors of HfO_2 and Si etching rates in $CF_4/O_2/Ar$ plasma provide the HfO_2/Si etching selectivity to be practically independent on gas mixing ratio. Figure 1(c) shows that, as the Ar fraction in the $CF_4/O_2/Ar$ gas mixture increases in the range of 0–50%, the HfO_2/Si etching selectivity keeps a near-to-constant average value of about 0.13. At the same time, the substitution of O_2 for Ar in $CHF_3/O_2/Ar$ gas mixture results in monotonically increasing HfO_2/Si etching selectivity in the range of 0.1–0.35. Therefore, in the investigated range of process conditions, both gas systems provide the rather close HfO_2/Si etching selectivities in O_2-rich plasmas, but show a noticeable difference in this parameter for Ar-rich plasmas.

From the above data, one can conclude that the understanding of the etching mechanisms in the given gas systems requires understanding of the reasons for the non-monotonic etching rates. Assuming HfO_2 etching mechanism in $CF_4/O_2/Ar$ and $CHF_3/O_2/Ar$ plasmas to be ion-assisted chemical reaction, one can select at least three general pathways explaining such phenomenon. These are:
(1) The non-monotonic behavior of ion energy flux and/or F atom flux. Particularly, Refs. [22, 31] reported the non-monotonic behavior in F atom density with variations of O_2 fraction in CF_4/O_2 plasmas, including the ICP system under the close range of experimental conditions. From Refs. [31, 32], it can be understood that an increase in F atom density up to 20–30% O_2 is provided by the stepwise dissociation of CF_x radicals due to their interactions with O and $O(^1D)$.
(2) The inconstancy of reaction probability for F atoms caused by increasing or decreasing fraction of the surface acceptable for their adsorption. For example, in our earlier works[21, 33] it was shown that, in the non-polymerizing plasmas, the non-monotonic etching rate can easily be obtained with monotonically decreasing flux of chemically active neutrals and monotonically increasing ion energy flux because the last causes an increase in reaction probability.
(3) The influence of gas mixing ratio on both formation and destruction kinetics for the fluorocarbon polymer layer. The first is closely connected with the flux of CF_x ($x = 1, 2$) radicals, while the last is determined by the ion energy flux, O atom flux and the H atom flux.[17, 19, 29]

All these issues will be analyzed below.

3.2. Plasma Parameters and Compositions

In order to obtain the data on plasma parameters, densities, and fluxes of active species, we used a combination of plasma diagnostics and modeling. Figure 2 represents the results of plasma diagnostics by Langmuir probes. From Figure 2(a), it can be seen that the substitution of O_2 for Ar results in increasing T_e in the ranges of 3.38–3.63 eV for $CF_4/O_2/Ar$ and 3.04–5.09 eV for $CHF_3/O_2/Ar$ plasma. The reason is a decrease in the electron energy loss for the low-threshold excitations (vibrational, electronic) of O_2 and other molecular species which appear in a gas phase as products of plasma chemical reactions. From Figures 2(a), (b) it can be seen also that both ion current density and total density of positive ions also show an increase toward Ar-rich plasmas. Particularly, for the

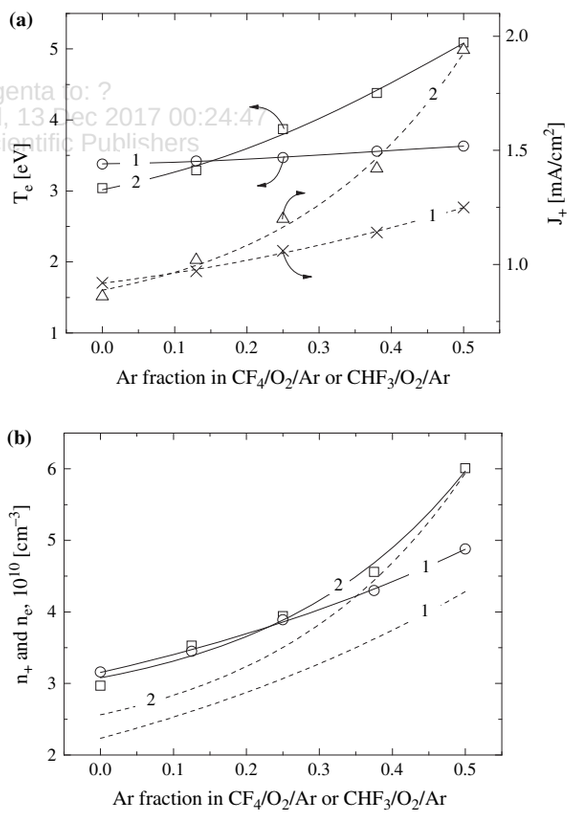

Figure 2. Measured and model-predicted plasma parameters in $CF_4/O_2/Ar$ (1) and $CHF_3/O_2/Ar$ (2) plasmas: (a) electron temperature (T_e) and ion current density (J_+); (b) total positive ion density (n_+, solid lines and symbols) and electron density (n_e, dashed lines). Process conditions correspond to Figure 1.

$CF_4/O_2/Ar$ gas mixture, an increase in the Ar content in a feed gas from 0–50% (i.e., the transition from CF_4/O_2 to CF_4/Ar system) results in $n_+ = 3.16 \times 10^{10}$–$4.88 \times 10^{10}$ cm^{-3} that corresponds to $J_+ =$ 0.92–1.25 mA/cm^2. The similar change in gas mixing ratios for $CHF_3/O_2/Ar$ plasma produces $n_+ = 2.97 \times 10^{10}$–$6.01 \times 10^{10}$ cm^{-3} and $J_+ = 0.86$–1.94 mA/cm^2. In our opinion, in both gas mixtures such effects are caused by a combination of two phenomena. First, an increasing T_e accelerates the ionization through the decreasing ionization rate coefficients for all types of neutral species. The high sensitivity of ionization rate coefficients to T_e is because of $\varepsilon_{iz} \approx 12$–$15$ eV $> (3/2)T_e$, where ε_{iz} is the threshold energy for ionization,[23, 24] and $(3/2)T_e$ is the mean electron energy. And secondly, the substitution of O_2 for Ar results in decreasing densities of electronegative species due to both O_2 itself and oxygen-containing reaction products. This suppresses the decay rates for positive ions and electrons through ion–ion recombination and dissociative attachment, respectively. The electron density in both gas mixtures follows the behavior of n_+ (Fig. 2(b)). The bigger gap between n_+ and n_e in $CF_4/O_2/Ar$ plasma (especially in the non-oxygenated gas mixture) is because of the higher electronegativity of this system ($n_-/n_e =$ 0.41–0.14 and 0.21–0.04 in $CF_4/O_2/Ar$ and $CHF_3/O_2/Ar$, respectively, at 0–50% Ar). This is connected with higher dissociative attachment rate coefficient for CF_x (x = 2–4) compared with both CHF_3 itself and HF as the dominant product of plasma chemical reactions.[24, 25] Therefore, the changes of gas mixing ratios in $CF_4/O_2/Ar$ and $CHF_3/O_2/Ar$ plasmas at a constant FC result in a quite similar effects on T_e and n_e. In fact, this means that the features of plasma compositions in these systems are mainly connected with the chemical properties of the original fluorocarbon molecules as well as with their reaction pathways with other "heavy" species.

Figure 3 illustrates the influence of Ar content in the $CF_4/Ar/O_2$ gas mixture on the densities of neutral species. It was found that, in the CF_4/O_2 gas system, the formation of F atoms is noticeably contributed by the stepwise channels involving F_2 (R15), FO (R23), CFO (R24) and CF_2O (R25). The acceleration of R15 compared with the non-oxygenated plasmas is due to increasing F_2 density ($n_{F_2} = 2.99 \times 10^{13}$–$6.84 \times 10^{11}$ cm^{-3} for 0–50% Ar) because of formation of these species in R73 and R76. The high formation rate and density of FO (6.23×10^{12}–8.18×10^{10} cm^{-3} for 0–38% Ar) are mainly provided by R40, R76 and R82. The high formation rate for the CFO species is provided by R25 and R75 while the CF_2O is effectively formed in R66, R71 and R72. Here, the total effect from the electron-impact dissociations of reaction products (R15, R23–R25) and atom-molecular reactions (R61–R63, R69) exceeds the formation rate of F atoms due to the dissociation of CF_4 in R7–R9. The substitution of O_2 for Ar at constant CF_4 fraction suppresses the F atom formation rate in mentioned stepwise pathways and simultaneously

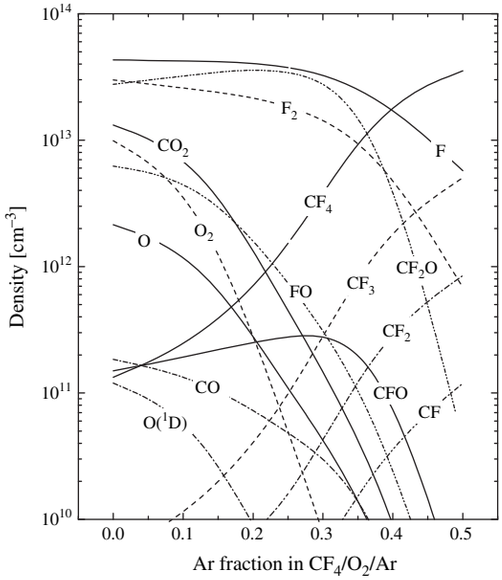

Figure 3. Model-predicted densities of neutral species in $CF_4/O_2/Ar$ plasma. Process conditions correspond to Figure 1.

accelerates R7–R9 due to increasing T_e (and thus, the dissociation rate coefficients), n_e, n_{CF_4} (1.33×10^{11}–3.53×10^{13} cm^{-3} for 0–50% Ar), and n_{CF_3} (5.21×10^{9}–5.04×10^{12} cm^{-3} for 0–50% Ar). The density of CF_3 radicals increases because of decreasing rates of their decompositions in R44, R45, R65 and R66 with the participation of O, O(^{1}D) and CFO. However, the increasing tendency for R7–R9 is weaker than the loss of F atom production in the stepwise reactions involving the oxygen-containing species. As a result, the substitution of O_2 for Ar in the $CF_4/Ar/O_2$ gas mixture under the given process conditions provides a continuous decrease in the total F atom formation rate and thus, in the F atom density.

Figure 4 shows the changes in the densities of neutral species in the $CHF_3/O_2/Ar$ plasma with the variable fraction of Ar in a feed gas. It can be seen that the main feature of this system is the domination of HF over other neutral species ($n_{HF} = 4.02 \times 10^{13} - 2.07 \times 10^{13}$ cm^{-3} for 0–50% Ar). In the non-oxygenated gas system (50% CHF_3+ 50% Ar) such situation is provided by the direct formation of HF from the original CHF_3 molecules in R3 as well as by the fast conversion of both CHF_3 and their first-step dissociation products, such as CF_3 and CHF_2, in atom-molecular reactions R26, R28, R29, R33, R34, R43 and R47. The contributions from the heterogeneous recombination of F and H atoms in R76 and R77 are noticeably lower. In the oxygenated plasmas, the HF formation appears to be higher due to the impacts of R39 and R60. The first is provided by the high density of F_2 molecules due to the same reasons as was described above for the CF_4-based plasmas. The second is connected with high density of molecular hydrogen which is effectively formed in R57 and R77. The high rate of R77 in the O_2-containing

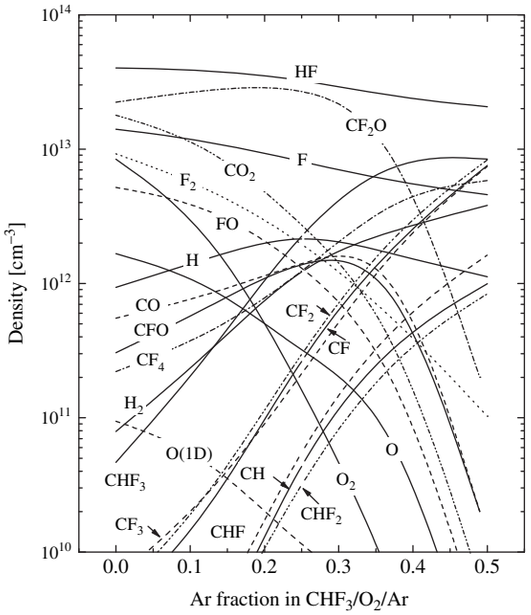

Figure 4. Model-predicted densities of neutral species in $CHF_3/O_2/Ar$ plasma. Process conditions correspond to Figure 1.

plasma is supported by the formation of H atoms in R32, R58 and R60. As a result, the substitution of O_2 for Ar in the $CHF_3/O_2/Ar$ gas mixture results in monotonically decreasing formation rate and density for HF molecules. Since the electron impact dissociations of HF (R14) and F_2 (R15) are the main formation mechanism for F atoms (the contribution of R25 with the participation of CF_2O is about twice lower due to lower rate coefficient), the behavior of n_F follows the monotonic changed of n_{HF} and n_{F_2}.

From the data of Figures 3 and 4, one can summarize the features of $CF_4/Ar/O_2$ and $CHF_3/O_2/Ar$ plasma influencing the chemical etching pathway:

(1) The $CF_4/Ar/O_2$ plasma provides the systematically higher F atom densities compared with the $CHF_3/O_2/Ar$ gas system. This fact is in good agreement with the experimental data published in Ref. [34]. Therefore, in the case if the etching process is not influenced by the fluorocarbon polymerization and is driven by the chemical etching pathway only, the CF_4-based plasma allows one to expect higher etching rates compared with the CHF_3-based one.

(2) The CHF_3-based plasma provides the systematically higher densities of CF_2 and CF radicals compared with the CF_4-based one. This means that, under the given set of experimental conditions, the CHF_3-based plasma is expected to be more polymerizing system. This conclusion is also in agreement with the previously published data.[18]

3.3. Etching Mechanism Approaches

From Refs. [21, 22, 35] it can be understood that, for the ion-assisted chemical reaction, the rate of the chemical etching pathway can be characterized by $\gamma_R\Gamma_F$, where Γ_F is the flux of F atoms, and γ_R is the reaction probability. For the given type of reaction product, $\gamma_R = \text{const}$ at constant surface temperature. In this case, the rate of chemical reaction is controlled by the Γ_F only. Accordingly, if the etching rate follows Γ_F, the neutral-flux-limited etching regime of the etching process takes place. Such situation is typical for the etching processes where the external factors (surface temperature, ion bombardment) provide the effective cleaning of the surface from the reaction products.[21] As can be seen from Figure 5(a), both gas systems provide the monotonically decreasing Γ_F toward Ar-rich plasmas. The maximum difference between these values (by about 3 times) appears in the completely oxygenated (50% FC + 50% O_2) plasmas.

The rate of the physical etching pathway is given by $Y_S\Gamma_+$, where $\Gamma_+ \approx J_+/e$ is the total flux of positive ions on

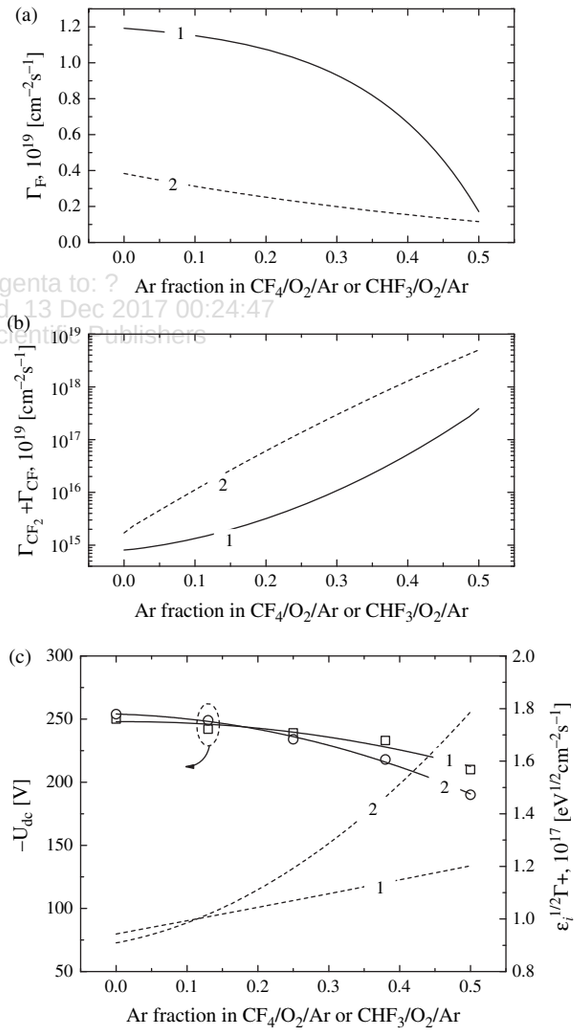

Figure 5. Fluxes of neutral and charged species in $CF_4/O_2/Ar$ (1) and $CHF_3/O_2/Ar$ (2) plasmas: (a) F atom fluxes (Γ_F); total fluxes of CF_2 and CF radicals ($\Gamma_{CF_2}+\Gamma_{CF}$); (c) ion energy fluxes ($\sqrt{\varepsilon_i}\Gamma$). Process conditions correspond to Figure 1.

the etched surface, and Y_s is the ion-type-averaged sputtering yield. For the ion bombardment energy $\varepsilon_i < 500$ eV, one can assume $Y_s \sim \sqrt{\varepsilon_i}$.[36] Therefore, the physical etching pathway can be characterized by the parameter $\sqrt{\varepsilon_i}\Gamma_+$ (so-called ion energy flux) where $\varepsilon_i \approx e|-U_f - U_{dc}|$. As can be seen from Figure 5(c), and increase in Ar fraction in both gas mixtures results in a quite close changes in negative dc bias voltage determining the ion bombardment energy. That is why the behaviors of ion energy fluxes in $CF_4/O_2/Ar$ and $CHF_3/O_2/Ar$ plasmas reflect both tendencies and the differences in J_+. Therefore, the maximum difference between CF_4-based and CHF_3-based plasmas in the parameters $\sqrt{\varepsilon_i}\Gamma_+$ appears in the non-oxygenated (50% FC + 50% Ar) systems while in the O_2-rich gas mixtures the corresponding values are very close.

From the comparison of Figures 1 and 5, one can conclude that the non-monotonic HfO_2 and Si etching rates do not correlate with both Γ_F and $\sqrt{\varepsilon_i}\Gamma_+$. This does not allow attributing the HfO_2 and Si etching mechanism to simple neutral-flux-limited or ion-flux-limited etching regimes. In our opinion, the situation for Si is much clearer than that for HfO_2. Really, since in the F-based gas chemistry the silicon is mainly etched by the chemical etching pathway,[17,18] a bit higher Si etching rate in CF_4/Ar gas system compared with CHF_3/Ar one reflects the differences in the fluxes of F atoms. Then, when the O_2 is added to the gas mixture, the Si etching rate in $CHF_3/O_2/Ar$ plasmas increases faster than that for $CF_4/O_2/Ar$, as it also predicted by the differences in Γ_F. The breaking of this rule in the completely oxygenated gas systems can be easily attributed to the higher $\sqrt{\varepsilon_i}\Gamma_+$ for $CHF_3/O_2/Ar$ plasma. This provides the better cleaning of the etched surface from reaction products and thus, leads to the greater increase in reaction probability compared with the $CF_4/O_2/Ar$ plasma. Therefore, one can conclude that the etching mechanism follows the "classical" scheme of ion-assisted chemical reaction in a transitional regime. Here, as was mentioned in Refs. [21, 33], the non-monotonic etching rate with increasing Ar fraction results from the concurrence of decreasing Γ_F and increasing the F atom reaction probability due to increasing $\sqrt{\varepsilon_i}\Gamma_+$.

As for the HfO_2, the situation looks as follows. Since the Hf fluorides are very low volatile compounds (the sublimation point for HfF_4 exceeds 900 °C),[37] one can surely expect the ion-flux limited etching regime, at least in the non-oxygenated plasmas. Here, the HfO_2 etching rate should be not sensitive to the differences in Γ_F, but should reflect the differences in $\sqrt{\varepsilon_i}\Gamma_+$. However, the last assumption seems to be not valid because the measured HfO_2 etching rate for CHF_3/Ar plasma is lower than that for CF_4/Ar plasma. This contradicts with the differences between corresponding ion energy fluxes shown in Figure 5(c). In our opinion, such contradiction may be connected with higher polymer formation rate in CHF_3/Ar plasma as follows from the data of Figure 5(b). When the O_2 is added to the gas mixture, the parameters $\Gamma_{CF_2} + \Gamma_{CF}$ determining the total flux of the polymer-forming species in both gas systems keep the near-to-constant gap and change in one and the same manner. Therefore, since the CHF_3-based plasma provides the systematically higher polymer growth rates at any Ar/O_2 mixing ratios, and the densities and fluxes of O atoms in both gas systems are rather close, the HfO_2 etching rates in the CHF_3-based plasma are systematically lower compared with the CF_4-based plasma. As for the non-monotonic behaviors of the HfO_2 etching rates vs. gas mixing ratio, the reasonable explanations of this phenomenon also involve the terms of polymer formation-decay kinetics. Since in both gas systems the transition to the Ar-rich gas mixtures leads to increasing polymer film growth rates, the non-monotonic etching rate with increasing Ar fraction in a feed gas can principally appear because of the concurrence between increasing Γ_F and decreasing Y_S due to the increasing thickness of the polymer layer. One more reason for obtaining the non-monotonic HfO_2 etching rate in the $CHF_3/O_2/Ar$ plasma may be connected with the effective destruction of polymer film due to the reactions of H atoms.[38] Really, Figure 3(b) shows that the H atom density (and thus, the flux of these species) in $CHF_3/O_2/Ar$ plasma has a non-monotonic behavior, and the position of the maximum is close to the for HfO_2 etching rate. However, the accurate understanding of HfO_2 etching mechanism needs additional investigations. The great support can come, for example, from the analysis of the chemical states of the etched surfaces in order to figure out the changes in surface densities of both reaction products and polymer-related groups.

4. CONCLUSION

In this work, we carried out the study of etching characteristics and mechanisms for HfO_2 and Si in $CF_4/O_2/Ar$ and $CHF_3/O_2/Ar$ inductively-coupled plasmas. The etching rates of HfO_2 thin films as well as the HfO_2/Si etching selectivities were measured as functions of Ar content in a feed gas (0–50% Ar) at fixed fluorocarbon gas content (50%), gas pressure (6 mTorr), input power (700 W), bias power (200 W), and total gas flow rate (40 sccm). Plasma parameters as well as the differences in plasma chemistries for CF_4- and CHF_3-based plasmas were analyzed using Langmuir probe diagnostics and 0-dimensional plasma modeling. These data allowed one to formulate the features of both gas systems influencing the etching processes in both neutral-flux-limited and ion-flux-limited etching regimes. It was found that, in both gas systems, the non-monotonic (with a maximum at about 15–20% Ar) HfO_2 etching rate does not correlate with monotonic changes of F atom flux and ion energy flux. It was proposed that, under the given set of experimental conditions, the HfO_2 etching process occurs in the ion-flux-limited mode of ion assisted chemical reaction and is affected by the factors determining the formation

and decomposition kinetics of the fluorocarbon polymer layer. The non-monotonic etching rate probably results from the concurrence of increasing Γ_+ and decreasing desorption yield for reaction products due to the increasing thickness of the polymer layer. The lower HfO_2 etching rates in $CHF_3/O_2/Ar$ plasma may be attributed to higher both polymer formation rate and polymer film thickness.

Acknowledgments: This work was supported by the Industrial Strategic Technology Development Program (10041681, Development of fundamental technology for 10 nm process semiconductors and 10 G size large area processes with high plasma density and VHF condition) funded by the Ministry of Knowledge Economy (MKE, Korea)

References and Notes

1. K. J. Hubbard and D. G. Schlom, *J. Mater. Res.* 11, 2757 (**1996**).
2. B. H. Lee, L. Kang, W.-J. Qi, R. Nieh, Y. Jeon, K. Onishi, and J. C. Lee, *Tech. Dig. Int. Electron Device Meet.*, Washington DC, USA (**1999**), p. 133.
3. S. Norasetthekul, P. Y. Park, K. H. Baik, K. P. Lee, J. H. Shin, B. S. Jeong, V. Shishodia, D. P. Norton, and S. J. Pearton, *Appl. Surf. Sci.* 187, 75 (**2002**).
4. K. Takahashi and K. Ono, *J. Vac. Sci. Technol. A* 24, 437 (**2006**).
5. K. S. Min, B. J. Park, S. W. Kim, S. K. Kang, G. Y. Yeom, S. H. Heo, H. S. Hwang, and C. Y. Kang, *J. Korean Phys. Soc.* 53, 1675 (**2008**).
6. J. Chen, W. J. Yoo, Z. Tan, Y. Wang, and D. S. H. Chan. *J. Vac. Sci. Technol. A* 22, 1552 (**2004**).
7. D. Shamiryan, M. Baklanov, M. Claes, W. Boullart, and V. Paraschiv. *Chem. Eng. Comm*. 196, 1475 (**2009**).
8. K. Takahashi, K. Ono, and Y. Setsuhara. *J. Vac. Sci. Technol. A* 23, 1691 (**2005**).
9. J. Anguita, M. Benedicto, R. Alvaro, B. Galiana, and P. Tejedor. *Jpn. J. Appl. Phys.* 49, 106504 (**2010**).
10. W. S. Hwang, J. Chen, W. J. Yoo, and V. Bliznetsov, *J. Vac. Sci. Technol. A* 23, 964 (**2005**).
11. M. H. Shin, S. W. Na, N. E. Lee, T. K. Oh, J. Y. Kim, T. H. Lee, and J. H. Ahn, *Jpn. J. Appl. Phys.* 44, 5811 (**2005**).
12. M. Kim, A. Efremov, H. W. Lee, H.-H. Park, M. P. Hong, N. K. Min, and K.-H. Kwon, *Thin Solid Films* 519, 6708 (**2011**).
13. J. Shoeb and M. J. Kushner. *J. Vac. Sci. Technol. A* 27, 1289 (**2009**).
14. D.-P. Kim, G.-H. Kim, J.-C. Woo, H.-J. Kim, C.-I. Kim, C.-I. Lee, S.-K. Lee, T.-W. Jung, S.-C. Moon, and S.-W. Park, *J. Korean Phys. Soc.* 54, 934 (**2009**).
15. D.-P. Kim, G.-H. Kim, J.-C. Woo, X. Yang, D.-S. Um, and C.-I. Kim, *Ferroelectrics* 381, 33 (**2009**).
16. P.-S. Kang, J.-C. Woo, Y.-H. Joo, and C.-I. Kim, *Vacuum* 93, 50 (**2013**).
17. J. W. Coburn, Plasma etching and reactive ion etching. New York, AVS Monograph Series (**1982**).
18. A. J. Roosmalen, J. A. G. Baggerman, and S. J. H. Brader, Dry etching for VLSI. Plenum Press, New-York (**1991**).
19. E. O. Johnson and L. Malter, *Phys. Rev.* 80, 58 (**1950**).
20. M. Sugavara, Plasma etching: Fundamentals and applications, Oxford University Press, New York (**1998**).
21. A. Efremov, N.-K. Min, B.-G. Choi, K.-H. Baek, and K.-H. Kwon, *J. Electrochem. Soc.* 155, D777 (**2008**).
22. A. M. Efremov, D.-P. Kim, and C.-I. Kim, *Vacuum* 75, 133 (**2004**).
23. T. Kimura and K. Ohe, *Plasma Sources Sci. Technol*. 8, 553 (**1999**).
24. P. Ho, J. E. Johannes, R. J. Buss, and E. Meeks, *J. Vac. Sci. Technol. A* 19, 2344 (**2001**).
25. D. Bose, M. V. V. S. Rao, T. R. Govindan, and M. Meyyappan, *Plasma Sources Sci. Technol.* 12, 225 (**2003**).
26. T. Kimura and M. Noto, *J. Appl. Phys.* 100, 063303 (**2006**).
27. D. Bose, S. Rauf, D. B. Hash, T. R. Govindan, and M. Meyyappan, *J. Vac. Sci. Technol. A*. 22, 2290 (**2004**).
28. NIST Chemical Kinetics Database http://kinetics.nist.gov/kinetics/index.jsp.
29. J. P. Barz, C. Oehr, and A. Lunk, *Plasma Process. Polym.* 8, 409 (**2011**).
30. M. A. Lieberman and A. J. Lichtenberg, Principles of plasma discharges and materials processing, John Wiley & Sons Inc., New York (**1994**).
31. I. C. Plumb and K. R. Ryan, *Plasma Chem. Plasma Proc.* 6, 205 (**1986**).
32. S. P. Venkatesan, I. Trachtenberg, and T. F. Edgar, *J. Electrochem. Soc.* 137, 2280 (**1990**).
33. A. M. Efremov, D. P. Kim, and C.-I. Kim, *IEEE Transactions on Plasma Science* 32, 1344 (**2004**).
34. M. T. Kim, *Journal of the Electrochemical Society* 149, G218-G225 (**2002**).
35. C. Lee, D. B. Graves, and M. A. Lieberman, *Plasma Chem. and Plasma Proc.* 16, 99 (**1996**).
36. B. Chapman, Glow Discharge Processes: Sputtering and Plasma Etching, John Wiley & Sons, New York (**1980**).
37. D. R. Lide, Handbook of Chemistry and Physics, CRC Press, New York (**1998-1999**).
38. L. Chen, L. Xu, D. Li, and B. Lin, *Microelectronic Engineering* 86, 2354 (**2009**).

Received: 3 January 2014. Accepted: 3 March 2014.